

Unusual Electronic Effects Imparted by Bridging Dinitrogen: an Experimental and Theoretical Investigation

Wesley A. Hoffert, Anthony K. Rappé, and Matthew P. Shores*

Department of Chemistry, Colorado State University, Fort Collins, Colorado 80523

Received July 29, 2010

We describe the preparation, structural and magnetic characterizations, and electronic structure calculations for a redox-related family of dinitrogen-bridged chromium acetylidy complexes containing the $[RC_2Cr(\mu-N_2)CrC_2R]^{n+}$ ($R = Ph-, ^1Pr_3Si-$; $n = 0, 1, 2$) backbone: $[(dmpe)_4Cr_2(C_2Ph)_2(\mu-N_2)]$ (**1**), $[(dmpe)_4Cr_2(C_2Si^1Pr_3)_2(\mu-N_2)]$ (**2**), $[(dmpe)_4Cr_2(C_2Si^1Pr_3)_2(\mu-N_2)]BAr^F_4$ (**3**), and $[(dmpe)_4Cr_2(C_2Si^1Pr_3)_2(\mu-N_2)](BAr^F_4)_2$ (**4**). Compounds **3** and **4** are synthesized via chemical oxidation of **2** with $[Cp_2Co]^+$ and $[Cp^*Fe]^+$, respectively. X-ray structural analyses show that the alteration of the formal Cr oxidation states does not appreciably change the Cr—N—N—Cr skeletal structures. Magnetic data collected for **2** and **4** are consistent with high-spin triplet and quintet ground states, respectively. The mixed-valent complex **3** exhibits temperature dependent magnetic behavior consistent with a quartet \rightleftharpoons doublet two-center spin equilibrium. Electronic structure calculations (B3LYP) performed on the full complexes in **2** and **4** suggest that the high-spin states arise from singly occupied orthogonal π^* orbitals coupled with a variable occupation of $d\delta$ orbitals. Significant N—N and Cr—N π -bonding pins the occupation of the π manifold, leading to variable occupation of the $d\delta$ space. In contrast, mixed-valent **3** is not well described by a B3LYP hybrid density functional model. A [9,11] CAS-SORCI study on a simplified model of **3** reproduces the observed Hund's rule violation for the $S=1/2$ ground state and places the lowest quartet 1.45 kcal/mol above the doublet ground state.

Introduction

A central focus of complex coordination chemistry is to ascertain the role(s) of bridging ligands in mediating metal–metal interactions. Advances in the areas of electron transfer, magnetic exchange, and small molecule activation can be attributed in large part to the results of fundamental studies carried out on model M–L–M systems.^{1–3} For example, the judicious choice of ligands to link paramagnetic metal centers has profound implications for the ability of a given complex to exist in a well-defined spin ground state.⁴ Thus, learning how simple ligands like oxo^{5–8} and cyanide^{9–14} manage exchange interactions has been critical to the development of molecular magnetism.

*To whom correspondence should be addressed. E-mail: shores@lamar.colostate.edu.

- (1) Richardson, D. E.; Taube, H. *Coord. Chem. Rev.* **1984**, *60*, 107–129.
- (2) Gunay, A.; Theopold, K. H. *Chem. Rev.* **2010**, *110*, 1060–1081.
- (3) Demadis, K. D.; Hartshorn, C. M.; Meyer, T. J. *Chem. Rev.* **2001**, *101*, 2655–2686.
- (4) *Single-Molecule Magnets and Related Phenomena*; Winpenny, R., Ed.; Springer: Berlin, 2006; Vol. 129.
- (5) Goodenough, J. B. *Phys. Rev.* **1955**, *100*, 564.
- (6) Weihe, H.; Gudel, H. U. *Inorg. Chem.* **1997**, *36*, 3632–3639.
- (7) Kanamori, J. *J. Phys. Chem. Solids* **1959**, *10*, 87–98.
- (8) Goldberg, D. P.; Caneschi, A.; Delfs, C. D.; Sessoli, R.; Lippard, S. J. *J. Am. Chem. Soc.* **1995**, *117*, 5789–5800.
- (9) Miyasaka, H.; Julve, M.; Yamashita, M.; Clérac, R. *Inorg. Chem.* **2009**, *48*, 3420–3437.

Metal complexes of another common bridging ligand, dinitrogen, are most often studied for their reactivity. While understanding the electronic structure of transition metal dinitrogen complexes is important for elucidating mechanistic aspects of N_2 activation, it is also critical to probing metal–metal electronic communication and its impact on magnetic communication and electron transfer. Dating from the 1970s,^{15,16} physical measurements on metal dinitrogen complexes have contributed significantly to our understanding of mixed valency as well as bridge-mediated/inner-sphere electron transfer processes.

The intramolecular magnetic interactions of paramagnetic $M_2(\mu_2-\eta^1:\eta^1-N_2)$ complexes including a tetrahedral $V^{III} \overset{\text{?}}{\underset{\text{?}}{\text{--}}} (\mu-N_2)$ complex¹⁷ and an octahedral $Cr^{I_2}(\mu-N_2)$ complex¹⁸

- (10) Toma, L. M.; Lescouezec, R.; Pasan, J.; Ruiz-Perez, C.; Vaissermann, J.; Cano, J.; Carrasco, R.; Wernsdorfer, W.; Lloret, F.; Julve, M. *J. Am. Chem. Soc.* **2006**, *128*, 4842–4853.
- (11) Sokol, J. J.; Hee, A. G.; Long, J. R. *J. Am. Chem. Soc.* **2002**, *124*, 7656–7657.
- (12) Entley, W. R.; Treadway, C. R.; Girolami, G. S. *Mol. Cryst. Liq. Cryst. Sci. Tech.* **1995**, *273*, 153–166.
- (13) Berlinguet, C. P.; Vaughn, D.; Cañada-Vilalta, C.; Galán-Mascarós, J. R.; Dunbar, K. R. *Angew. Chem., Int. Ed.* **2003**, *42*, 1523–1526.
- (14) Li, D.; Parkin, S.; Wang, G.; Yee, G. T.; Clérac, R.; Wernsdorfer, W.; Holmes, S. M. *J. Am. Chem. Soc.* **2006**, *128*, 4214–4215.
- (15) Magnuson, R. H.; Taube, H. *J. Am. Chem. Soc.* **1972**, *94*, 7213–7214.
- (16) Richardson, D. E.; Sen, J. P.; Buhr, J. D.; Taube, H. *Inorg. Chem.* **1982**, *21*, 3136–3140.

have been interpreted in terms of weak antiferromagnetic coupling. In light of the similarity of dinitrogen to the iso-electronic cyanide bridging ligand, this model makes intuitive sense.¹² However, recent investigations involving N₂-bridged transition metal complexes indicate that non-diamagnetic, high spin electronic ground states exist for tetrahedral Mo^{III}₂(μ-N₂)¹⁹ and trigonal planar Co^I₂(μ-N₂) complexes.²⁰ To correspond with the antiferromagnetic terminology employed by others, we loosely refer to these non-diamagnetic ground states as “ferromagnetically coupled”; however, a more accurate description would invoke an electronic structure similar to the triplet ground state of dioxygen. The electronic structure that accounts for high spin magnetic behavior in a formally Fe^I₂(μ-N₂) complex has been described in terms of strong direct antiferromagnetic coupling between Fe^{II} and a diazenido (N₂²⁻) bridging ligand.^{21–23} Recent theoretical calculations involving a Ni^I₂(μ-N₂) complex predict a triplet ground state, although magnetic measurements made in solution are consistent with the presence of two weakly- or non-coupled S = 1/2 Ni^I ions.²⁴ There, stepwise potassium metal reduction of the Ni₂ complex occurs at the dinitrogen ligand, and metal–ligand antiferromagnetic coupling is invoked to account for the diamagnetism observed in the di-reduced K₂Ni₂(μ-N₂) species.

It is clear from the available reports that interpretations of the measured magnetic properties of dinitrogen-bridged complexes are varied. One source of difficulty is that the few structurally characterized paramagnetic M–N–N–M complexes display myriad coordination geometries as well as a variety of valence bond structures and electron counts, which surely have profound implications for magnetic communication. On a case-by-case basis, magneto-structural correlations drawn from comparisons of metal dinitrogen complexes have been consistent with the theory of the day.^{17,25–27} However, a more detailed magneto-structural and theoretical survey of multiple metal dinitrogen complexes with comparable structures but with different electron counts should allow for the drawing of a more complete picture of dinitrogen-mediated magnetic properties, and ultimately lead to a deeper understanding of metal dinitrogen complex electronic structures.

From a theoretical standpoint, we have been interested for some time in the electronic structures underpinning dinitrogen activation^{28,29} as well as bridge-mediated magnetism.^{30–32}

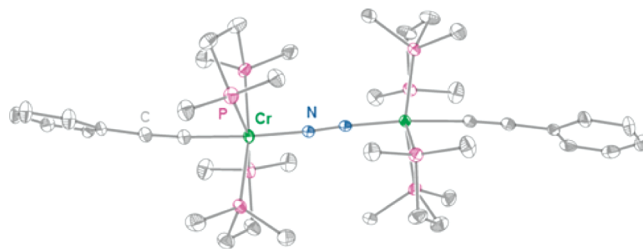


Figure 1. Structure of **1** rendered with 40% ellipsoids. Green, violet, dark blue and gray ellipsoids represent Cr, P, N, and C atoms, respectively. Hydrogen atoms are omitted for clarity.

Our synthetic entry is more recent: in an effort to synthesize paramagnetic transition metal ethynylbenzene complexes³³ for single-molecule magnet investigations,^{4,34,35} our explorations of low valent chromium acetylidy chemistry led to the isolation of a dinitrogen-bridged dinuclear Cr^I acetylidy complex (**1**, Figure 1).

The (trimethylsilyl)acetylidy analogue of this complex was reported recently by Berben and Kozimor.^{18,36} There, the magnetic susceptibility data for that complex were fit to a model where S = 1/2 centers weakly couple antiferromagnetically. Cyclic voltammograms obtained for the Me₃Si-containing complex indicated that the oxidized product(s) were stable on the electrochemical time scale. Further, density functional calculations performed on a neutral model complex offered a forecast of a *weakened* dinitrogen bond upon *oxidation* of the Cr^I centers.¹⁸

Intrigued by the potential for redox changes to influence dinitrogen activation, we have set out to isolate and study the [RC₂Cr(μ-N₂)CrC₂R]ⁿ⁺ species in all its chemically available oxidation states. More generally, the work is motivated by the opportunity to establish magneto-structural and electronic correlations in transition metal complexes bridged by small ligands, which in turn can benchmark theoretical modeling for species with tailored magnetic and electronic properties. Herein, we report the syntheses, characterizations, and initial computational investigations of a structurally related family of [RC₂Cr(μ-N₂)CrC₂R]ⁿ⁺ (R = Ph, iPr₃Si; n = 0, 1, 2) species, where redox tuning gives rise to significant changes in magnetism, but negligible alteration of the dinitrogen moiety. As will be shown below, experimental data from all three compounds is necessary to *begin* to understand the changes in electronic structure brought about by redox events.

Experimental Section

Preparation of Compounds. Manipulations were performed either inside a dinitrogen-filled glovebox (MBRAUN Labmaster 130) or via Schlenk techniques on dinitrogen manifolds. Pentane was distilled over sodium metal and subjected to three freeze–pump–thaw cycles. Other solvents were sparged with dinitrogen,

- (17) Ferguson, R.; Solari, E.; Floriani, C.; Osella, D.; Ravera, M.; Re, N.; Chiesi-Villa, A.; Rizzoli, C. *J. Am. Chem. Soc.* **1997**, *119*, 10104–10115.
- (18) Berben, L. A.; Kozimor, S. A. *Inorg. Chem.* **2008**, *47*, 4639–4647.
- (19) Curley, J. J.; Cook, T. R.; Reece, S. Y.; Müller, P.; Cummins, C. C. *J. Am. Chem. Soc.* **2008**, *130*, 9394–9405.
- (20) Ding, K.; Pierpont, A. W.; Brennessel, W. W.; Lukat-Rodgers, G.; Rodgers, K. R.; Cundari, T. R.; Bill, E.; Holland, P. L. *J. Am. Chem. Soc.* **2009**, *131*, 9471–9472.
- (21) Smith, J. M.; Sadique, A. R.; Cundari, T. R.; Rodgers, K. R.; Lukat-Rodgers, G.; Lachicotte, R. J.; Flaschenriem, C. J.; Vela, J.; Holland, P. L. *J. Am. Chem. Soc.* **2006**, *128*, 756–769.
- (22) Stoian, S. A.; Vela, J.; Smith, J. M.; Sadique, A. R.; Holland, P. L.; Münck, E.; Bominaar, E. L. *J. Am. Chem. Soc.* **2006**, *128*, 10181–10192.
- (23) Holland, P. L. *Acc. Chem. Res.* **2008**, *41*, 905–914.
- (24) Pfirrmann, S.; Limberg, C.; Herwig, C.; Stösser, R.; Ziemer, B. *Angew. Chem., Int. Ed.* **2009**, *48*, 3357–3361.
- (25) Chatt, J.; Fay, R. C.; Richards, R. L. *J. Chem. Soc. A* **1971**, 702–704.
- (26) Treitel, I. M.; Flood, M. T.; Marsh, R. E.; Gray, H. B. *J. Am. Chem. Soc.* **1969**, *91*, 6512–6513.
- (27) Sellmann, D. *Angew. Chem., Int. Ed. Engl.* **1974**, *13*, 639–649.
- (28) Rappé, A. K. *Inorg. Chem.* **1984**, *23*, 995–996.
- (29) Rappé, A. K. *Inorg. Chem.* **1986**, *25*, 4686–4691.
- (30) Hart, J. R.; Rappé, A. K.; Gorun, S. M.; Upton, T. H. *Inorg. Chem.* **1992**, *31*, 5254–5259.

- (31) Hart, J. R.; Rappé, A. K.; Gorun, S. M.; Upton, T. H. *J. Phys. Chem.* **1992**, *96*, 6255–6263.

- (32) Hart, J. R.; Rappé, A. K.; Gorun, S. M.; Upton, T. H. *J. Phys. Chem.* **1992**, *96*, 6264–6269.

- (33) Weyland, T.; Costuas, K.; Mari, A.; Halet, J. F.; Lapinte, C. *Organometallics* **1998**, *17*, 5569–5579.

- (34) Sessoli, R.; Gatteschi, D.; Caneschi, A.; Novak, M. A. *Nature* **1993**, *365*, 141–143.

- (35) Milios, C. J.; Vinslava, A.; Wernsdorfer, W.; Moggach, S.; Parsons, S.; Perlepes, S. P.; Christou, G.; Brechin, E. K. *J. Am. Chem. Soc.* **2007**, *129*, 2754–2755.

- (36) Berben, L. A. Ph.D. Thesis, University of California, Berkeley, CA, 2005.

Table 1. Crystallographic Data^a for Compounds $[(\text{dmpe})_4\text{Cr}_2(\text{PhC}_2)_2(\mu\text{-N}_2)] \cdot \text{C}_6\text{H}_{12}$ (**1**· C_6H_{12}), $[(\text{dmpe})_4\text{Cr}_2(\text{iPr}_3\text{SiC}_2)_2(\mu\text{-N}_2)]$ (**2**), $[(\text{dmpe})_4\text{Cr}_2(\text{iPr}_3\text{SiC}_2)_2(\mu\text{-N}_2)]\text{BAr}^{\text{F}}_4 \cdot 1.5 \text{Et}_2\text{O}$ (**3**· $1.5\text{Et}_2\text{O}$), $[(\text{dmpe})_4\text{Cr}_2(\text{iPr}_3\text{SiC}_2)_2(\mu\text{-N}_2)]\text{BAr}^{\text{F}}_4$ (**3**), and $[(\text{dmpe})_4\text{Cr}_2(\text{iPr}_3\text{SiC}_2)_2(\mu\text{-N}_2)](\text{BAr}^{\text{F}}_4)_2 \cdot 3.5 \text{THF}$ (**4**· 3.5THF)

	1 · C_6H_{12}	2	3 · $1.5\text{Et}_2\text{O}$ (100 K)	3 (296 K)	4 · 3.5THF
formula	$\text{C}_{46}\text{H}_{86}\text{Cr}_2\text{N}_2\text{P}_8$	$\text{C}_{46}\text{H}_{104}\text{Cr}_2\text{N}_2\text{P}_8\text{Si}_2$	$\text{C}_{84}\text{H}_{133}\text{BCr}_2\text{F}_{24}\text{N}_2\text{P}_8\text{Si}_2\text{O}_{1.5}$	$\text{C}_{78}\text{H}_{118}\text{BCr}_2\text{F}_{24}\text{N}_2\text{P}_8\text{Si}_2$	$\text{C}_{124}\text{H}_{158}\text{B}_2\text{Cr}_2\text{F}_{48}\text{N}_2\text{P}_8\text{Si}_2\text{O}_{3.5}$
M_r	1018.93	1093.25	2069.67	1958.49	3072.98
T (K)	100(2)	100(2)	100(2)	296(2)	100(2)
space group	$P2_1/c$	$Pbca$	$P2_1/c$	$P2_1/c$	$P\bar{1}$
a (Å)	12.3602(2)	18.0902(5)	14.5070(4)	14.6116(6)	14.2386(5)
b (Å)	12.7197(2)	19.6306(5)	29.6682(9)	30.4203(13)	17.1753(6)
c (Å)	34.7651(6)	34.351(1)	24.1919(7)	24.9312(10)	31.8445(11)
α (deg)	90	90	90	90	88.101(2)
β (deg)	93.298(1)	90	96.531(2)	96.848(2)	86.562(2)
γ (deg)	90	90	90	90	69.587(2)
V (Å ³)	5457.0(2)	12198.8(6)	10344.5(5)	11002.6(8)	7248.8(4)
Z	4	8	4	4	2
R_{int}	0.075	0.094	0.063	0.060	0.068
$R1^b$ ($I > 2\sigma(I)$)	0.046	0.062	0.065	0.077	0.093
$wR2^c$ (all data)	0.113	0.180	0.209	0.220	0.277

^a Obtained with graphite-monochromated Mo Kα ($\lambda = 0.71073$ Å) radiation. ^b $R1 = \sum ||F_o| - |F_c|| / \sum |F_o|$. ^c $wR2 = \{\sum w(F_o^2 - F_c^2)^2 / \sum w(F_o^2)\}^{0.5}$.

passed over activated alumina, and degassed prior to use. The preparation of $[(\text{dmpe})_2\text{CrCl}_2]$ ($\text{dmpe} = 1,2\text{-bis(dimethylphosphino)-ethane}$) has been described elsewhere.³⁷ The reagent $[\text{CoCp}_2]\text{BAr}^{\text{F}}_4$ ($\text{BAr}^{\text{F}}_4 = \text{tetrakis(3,5-bis(trifluoromethylphenyl)borate)}$) was made by PF_6^- anion metathesis in a manner analogous to the preparation of $[\text{Cp}_2^*\text{Fe}]\text{BAr}^{\text{F}}_4$.³⁸ All other reagents were purchased commercially and were used without further purification.

[(dmpe)₄Cr₂(C₂Ph)₂(μ-N₂)] (1). A solution of $[(\text{dmpe})_2\text{CrCl}_2]$ (100 mg, 0.236 mmol) in 5 mL of tetrahydrofuran (THF) at -78°C was added to a mixture of phenylacetylene (26 μL , 0.24 mmol) and *n*-BuLi (0.33 mL of a 1.59 M solution in hexanes, 0.53 mmol) in 20 mL of pentane at -78°C . The green mixture was warmed to 293 K, resulting in a color change to brown. After stirring for 1 h, the solvent was removed in vacuo, and the residue was extracted with 25 mL of a 10% (v/v) methylcyclopentane/hexanes solution. The brown solution was concentrated to about 15 mL and was placed in a -40°C freezer for 1 day, resulting in the precipitation of dark brown needle crystals suitable for X-ray analysis. The crystals were isolated by filtration, washed with cold (-40°C) pentane (3×2 mL), and dried under dinitrogen to afford the final product (13 mg, 0.014 mmol, 12%). Absorption spectrum (toluene): $\lambda_{\text{max}} (\varepsilon_M)$ 317 (12300), 441 (10400), 543 (sh, 4100), 955 nm (6800 $\text{M}^{-1}\cdot\text{cm}^{-1}$). IR (solid, mineral oil): ν_{CC} 2027 cm^{-1} . Raman (solution in C_6H_6): ν_{NN} 1685 cm^{-1} . ¹H NMR (C_6D_6) δ 20.50 (br, 10H, Ar-H), -3.05 (br, 24H, -PCH₃), -4.56 (br, 8H, -PCH₂), -19.23 (br, 24H, -PCH₃), -22.51 ppm (br, 24H, -PCH₂). Anal. calcd. for $\text{C}_{40}\text{H}_{74}\text{N}_2\text{Cr}_2\text{P}_8$: C, 51.38; H, 7.98; N, 3.00. Found: C, 51.70; H, 7.85; N, 2.67.

[(dmpe)₄Cr₂(C₂Si*i*Pr₃)₂(μ-N₂)] (2). A solution of $[(\text{dmpe})_2\text{CrCl}_2]$ (515 mg, 1.22 mmol) in 10 mL of THF at -78°C was added to a mixture of triisopropylsilylacetylene (0.27 mL, 1.22 mmol) and *n*-BuLi (1.77 mL of a 1.59 M solution on hexanes, 2.79 mmol) in 20 mL of pentane at -78°C . As the green mixture was slowly warmed to 293 K, the color changed to dark red-orange. After stirring for 1 h, the solvent was removed in vacuo overnight, and the residue was extracted with 20 mL of pentane and filtered through Celite. The red-orange solution was concentrated to about 10 mL and was placed in a -40°C freezer for crystallization. After 1 day, dark red needle crystals formed. The crystals were isolated by filtration, washed with cold (-40°C) pentane (2×2 mL), and dried under dinitrogen to afford 110 mg of the final product (0.100 mmol, 17%). Crystals suitable for X-ray analysis were obtained by cooling a dilute solution of **2** in

pentane at -40°C for 3 days. Absorption spectrum (toluene): $\lambda_{\text{max}} (\varepsilon_M)$ 427 (44900), 940 nm (30300 $\text{M}^{-1}\cdot\text{cm}^{-1}$). IR (solid, mineral oil): ν_{CC} 1944, ν_{CSi} 833 cm^{-1} . Raman (solution in C_6H_6): ν_{NN} 1680 cm^{-1} . ¹H NMR (C_6D_6) δ 2.16 (br, 50H, -PCH₂ and -Si(C₃H₇)₃), -3.71 (br, 24H, -PCH₃), -4.60 (br sh, 8H, -PCH₂), -19.95 ppm (br, 24H, -PCH₃). Anal. Calcd. for $\text{C}_{46}\text{H}_{106}\text{N}_2\text{Cr}_2\text{P}_8\text{Si}_2$: C, 50.44; H, 9.75; N, 2.56. Found: C, 50.28; H, 9.68; N, 2.28.

[(dmpe)₄Cr₂(C₂Si*i*Pr₃)₂(μ-N₂)]BAr^F₄ (3). To a stirred solution of **2** (30 mg, 0.027 mmol) in 3 mL of diethyl ether was added a solution of $[\text{Cp}_2\text{Co}]\text{BAr}^{\text{F}}_4$ (28.8 mg, 0.027 mmol) in 3 mL of diethyl ether. The solution immediately turned dark green. After stirring for 5 min, the solution was filtered through a plug of Celite. Pentane (10 mL) was added, and the solution was cooled to -40°C . After 1 day, dark green needle crystals formed. The crystals were isolated by filtration, washed with pentane (2×10 mL), and dried under dinitrogen to afford 38 mg (0.019 mmol, 71%) of product. X-ray quality parallelepiped crystals of **3**· $1.5\text{Et}_2\text{O}$ were grown by layering pentane over a concentrated solution of **3** in diethyl ether in a -40°C freezer for 2 days. Absorption spectrum (diethyl ether): $\lambda_{\text{max}} (\varepsilon_M)$ 343 (10410), 361 (10590), 408 (8850), 607 (780), 914 nm (3180 $\text{M}^{-1}\cdot\text{cm}^{-1}$). IR (solid, mineral oil): ν_{CC} 1963, ν_{CSi} 838 cm^{-1} . Anal. Calcd. for $\text{C}_{82}\text{H}_{128}\text{N}_2\text{Cr}_2\text{BF}_{24}\text{P}_8\text{Si}_2\text{O}$ (**3**· Et_2O): C, 48.45; H, 6.35; N, 1.38. Found: C, 48.34; H, 6.41; N, 1.23. Crystals maintained at room temperature release varying amounts of Et_2O ; samples used for magnetic studies were ground finely, releasing all solvate molecules.

[(dmpe)₄Cr₂(C₂Si*i*Pr₃)₂(μ-N₂)](BAr^F₄)₂ (4). To a stirred solution of **2** (40 mg, 0.037 mmol) in 10 mL of diethyl ether was added a solution of $[\text{Cp}_2^*\text{Fe}]\text{BAr}^{\text{F}}_4$ (86.9 mg, 0.073 mmol) in 5 mL of diethyl ether. The solution first turned green, then dark brown. After stirring for 5 min, the solution was filtered through Celite. Pentane (ca. 20 mL) was added to precipitate a brown solid. The solid was isolated by filtration and washed with pentane (2×10 mL) to remove any trace of $[\text{Cp}_2^*\text{Fe}]$, yielding 75 mg (0.027 mmol, 73%) of product. X-ray quality parallelepiped crystals of **4**· 3.5THF were grown by layering pentane over a concentrated solution of **4** in THF in a -40°C freezer for 2 days. Absorption spectrum (diethyl ether): $\lambda_{\text{max}} (\varepsilon_M)$ 349 (10440), 446 (5280), 904 nm (7000 $\text{M}^{-1}\cdot\text{cm}^{-1}$). IR (solid, mineral oil): ν_{CC} 1982, ν_{CSi} 838 cm^{-1} . Raman (THF): ν_{NN} 1710 cm^{-1} . Anal. Calcd. for $\text{C}_{110}\text{H}_{130}\text{N}_2\text{B}_2\text{Cr}_2\text{F}_{48}\text{P}_8\text{Si}_2$: C, 46.80; H, 4.65; N, 0.99. Found: C, 46.67; H, 4.74; N, 0.90.

X-ray Structure Determinations. All compounds reported herein were characterized by single crystal X-ray analysis (Table 1). Single crystals were coated in Paratone oil prior to removal from the glovebox. Crystals to be investigated at low temperature were supported on Cryoloops, then mounted on a Bruker

(37) Girolami, G. S.; Wilkinson, G.; Galas, A. M. R.; Thorntonpett, M.; Hursthouse, M. B. *J. Chem. Soc., Dalton Trans.* **1985**, 1339–1348.

(38) Chávez, I.; Alvarez-Carena, A.; Molins, E.; Roig, A.; Maniukiewicz, W.; Arancibia, A.; Arancibia, V.; Brand, H.; Manríquez, J. M. *J. Organomet. Chem.* **2000**, *601*, 126–132.

Table 2. Selected Measured and Calculated (comp) Interatomic Distances (\AA) and Angles (deg) for the Structures of $[(\text{dmpe})_4\text{Cr}_2(\text{iPr}_3\text{SiC}_2)_2(\mu\text{-N}_2)]$ (**2**), $[(\text{dmpe})_4\text{Cr}_2(\text{iPr}_3\text{SiC}_2)_2(\mu\text{-N}_2)](\text{BAR}^{\text{F}}_4)\cdot 1.5\text{Et}_2\text{O}$ (**3**·1.5Et₂O), **3**, and $[(\text{dmpe})_4\text{Cr}_2(\text{iPr}_3\text{SiC}_2)_2(\mu\text{-N}_2)](\text{BAR}^{\text{F}}_4)\cdot 3.5\text{THF}$ (**4**·3.5THF)

	2	2 (comp)	3 ·1.5Et ₂ O (100 K)	3 (296 K)	3 (comp)	4 ·3.5THF	4 (comp)
Cr—N	1.881[2] ^b	1.929	1.857[7]	1.887[5]	2.050	1.88[1]	1.925
N≡N	1.187[5]	1.183	1.195[5]	1.164[3]	1.156	1.181[8]	1.185
Cr—C	2.053[2]	2.090	2.051[8]	2.041[6]	2.044	2.054[3]	2.054
Cr···Cr	4.946[3]	5.038	4.9083[10]	4.9362[8]	5.256	4.9313[15]	5.034
C≡C	1.231[4]	1.244	1.220[4]	1.223[6]	1.242	1.216[4]	1.240
C—Si	1.815[3]	1.842	1.85[1]	1.82[2]	1.838	1.842[1]	1.875
Cr—P	2.32[3]	2.32 ^a	2.35[1]	2.37[2]	2.35 ^a	2.42[2]	2.42 ^a
P—Cr—N	96.1[8]	95.90	97[2]	96[2]	94.99	96[2]	96.58
P—Cr—C	84[1]	84.11	83[2]	84[1]	85.01	84[2]	83.42
C—Cr—N	178.2[5]	179.28	178.15[8]	177[1]	179.22	178.8[9]	179.12
Cr—N≡N	179.0[4]	179.34	178.0[3]	177.5[2]	179.66	178[1]	179.27
Cr—C≡C	178[2]	179.13	179.0[5]	178.9[8]	178.91	178.3[7]	178.78
C≡C—Si	176[1]	178.15	175.8[4]	178.7[3]	178.54	178[1]	178.61
dmpe—Cr(1)—N	97.8[5]		99.2[4]	98.2[5]		98.5[4]	
dmpe—Cr(2)—N	97.9[5]		99.8[4]	99[1]		98.5[4]	

^aThe Cr—P distances were constrained to be the same as those from the X-ray structure. ^bSquare brackets [] represent esds for averaged metric parameters.

Kappa Apex 2 CCD diffractometer under a stream of cold dinitrogen. For the room-temperature data set for **3**, the crystal was encased in epoxy and supported on a glass fiber before being mounted on the diffractometer under a stream of dinitrogen maintained at 296 K. All data collections were performed with Mo K α radiation and a graphite monochromator. Initial lattice parameters were determined from a minimum of 189 reflections harvested from 36 frames, and data sets were collected with complete coverage and 4-fold redundancy. Data were integrated and corrected for absorption effects with the Apex 2 software package.³⁹ Structures were solved by direct methods and refined against | F^2 | with the SHELXTL software package.⁴⁰ Thermal parameters for all non-H atoms were refined anisotropically with the exception of disordered C, P, and F atoms as noted in the respective cif files. Hydrogen atoms were added at the ideal positions and were refined using a riding model where the thermal parameters were set at 1.2 times those of the attached carbon atom (1.5 times for methyl carbons).

Magnetic Susceptibility Measurements. Magnetic susceptibility data were collected with a Quantum Design MPMS-XL SQUID magnetometer. Samples were loaded into gelatin capsules and inserted into straws prior to analysis. The straws were sealed in plastic bags prior to removal from the glovebox, and were quickly loaded into the instrument to minimize exposure to air. Diamagnetic corrections were applied by using Pascal's constants and by subtracting the diamagnetic susceptibility from an empty sample holder. Susceptibility data were fit with theoretical models using a relative error minimization routine (julX 1.41).⁴¹ Zero field splitting parameters obtained with julX are based on the spin Hamiltonian

$$\hat{H} = \sum_{i=1}^{ns} D_i [S_{z,i}^2 - 1/3S_i(S_i+1) + E_i/D_i(S_{x,i}^2 - S_{y,i}^2)] + \sum_{i=1}^{ns} g\beta\vec{S}_i \cdot \vec{B}$$

Fits of the magnetization data were obtained with the ANISOFIT⁴² program and are based on the spin Hamiltonian $\hat{H} = D\hat{S}_z^2 + E(\hat{S}_x^2 + \hat{S}_y^2) + g_{iso}\beta\vec{S} \cdot \vec{B}$.

(39) APEX 2; Bruker Analytical X-Ray Systems, Inc.: Madison, WI, 2008.

(40) Sheldrick, G. M. SHELXTL; Bruker Analytical X-Ray Systems, Inc.: Madison, WI, 1999.

(41) Bill, E. *julX*, 1.41; Max Planck Institute for Bioinorganic Chemistry: Mülheim an der Ruhr, Germany, 2008 (http://www.mpi-muelheim.mpg.de/bac/login/bill/julX_en.php).

(42) Shores, M. P.; Sokol, J. J.; Long, J. R. *J. Am. Chem. Soc.* **2002**, *124*, 2279–2292.

Other Physical Measurements. UV-vis absorption spectra were obtained with a Hewlett-Packard 8453 spectrophotometer in airfree cuvettes. Vis-Near IR spectra were recorded using a Cary 500 spectrophotometer. IR spectra were measured with a Nicolet 380 FT-IR using mineral oil mulls sandwiched between NaCl plates. ¹H NMR spectra were recorded using a Varian INOVA instrument operating at 300 MHz. EPR spectra were obtained using a continuous wave X-band Bruker EMX 200U instrument outfitted with a liquid nitrogen cryostat. Raman spectra were acquired with a Nicolet 760 spectrometer equipped with an FT-Raman module using an incident laser wavelength of 1064 nm. Cyclic voltammetry was done in 0.1 M solutions of (Bu₄N)PF₆ in THF unless otherwise noted. The voltammograms were recorded with a CH Instruments potentiostat (either model 1230A or 660C) using a 0.25 mm Pt disk working electrode, Ag/Ag⁺ reference electrode, and a Pt mesh auxiliary electrode. All voltammograms shown were measured with a scan rate of 0.1 V/s. Reported potentials are referenced to the [Cp₂Fe]⁺/[Cp₂Fe] redox couple and were determined by adding ferrocene as an internal standard at the conclusion of each electrochemical experiment. Elemental analyses for compounds **1**, **2**, and **4** were performed by Robertson Microlit Laboratories in Madison, NJ. The elemental analysis for **3** was performed by the microanalytical laboratory at the University of California at Berkeley.

Electronic Structure Calculations. Restricted and unrestricted B3LYP hybrid density functional studies⁴³ were carried out in the G03 suite of electronic structure codes.⁴⁴ Geometry optimized structures for the triplet, quartet, and quintet states of **2**, **3**, and **4** utilized the X-ray coordinates for **2**, **3**·1.5 Et₂O, and **4**·3.5 THF as initial input (sp³ C—H bond distances adjusted to 1.096 Å and sp² C—H bonds adjusted to 1.090 Å). Metric parameters are collected in Table 2 and calculated coordinates are provided as Supporting Information. The LANL2⁴⁵ basis sets and effective core potentials were used for Si, P, and Cr; H, C, and N were described with a 6-31 g* model.^{46–49} ORCA⁵⁰

(43) Becke, A. D. *J. Chem. Phys.* **1993**, *98*, 5648.

(44) Frisch, M. J. et al. *Gaussian 03*; Gaussian, Inc.: Wallingford, CT, 2004.

(45) Hay, P. J.; Dunning, T. H. *J. Chem. Phys.* **1976**, *64*, 5077.

(46) Ditchfield, R.; Hehre, W. J.; Pople, J. A. *J. Chem. Phys.* **1971**, *54*, 724.

(47) Hehre, W. J.; Ditchfield, R.; Pople, J. A. *J. Chem. Phys.* **1972**, *56*, 2257.

(48) Binkley, J. S.; Pople, J. A.; Hehre, W. J. *J. Am. Chem. Soc.* **1980**, *102*, 939.

(49) Franci, M. M.; Pietro, W. J.; Hehre, W. J.; Binkley, J. S.; Gordon, M. S.; DeFrees, D. J.; Pople, J. A. *J. Chem. Phys.* **1982**, *77*, 3654.

(50) ORCA is a modern electronic structure program package written by F. Neese, with contributions from Becker, U.; Ganiouchine, D.; Kossmann, S.; Petrenko, T.; Ripplinger, C.; Wennmohs, F.; .

CAS-SORCI computations used smaller models of compounds **3** and **4** (**3***, **4***) wherein the dmpe methyl and acetylide $^3\text{Pr}_3\text{Si}$ substituents were replaced with hydrogens directed along the P–C and C–Si bond vectors with P–H and C–H bond distances of 1.42 and 1.06 Å, respectively. The CAS-SORCI computations did not utilize effective core potentials, and the 6-31 g basis set was used for all atoms except Cr. For Cr the Ahlrichs-DZ basis⁵¹ was used. B3LYP UKS quintet spin natural orbitals for **4*** were used as a starting guess for a [9,11] CAS calculation on **3*** that equally weighted the lowest two doublet states as well as the lowest two quartets. This model was chosen to prevent artificial symmetry breaking and provide an unbiased reference space for the subsequent CI/perturbation theory step.

Results

Syntheses and Characterizations of the $[\text{RC}_2\text{Cr}(\mu\text{-N}_2)\text{CrC}_2\text{R}]^{n+}$ Complexes. It has been shown that $[(\text{dmpe})_2\text{Cr}^{\text{II}}(\text{C}_2\text{R})_2]$ complexes can be prepared by addition of 2 equiv of LiC₂R to $[(\text{dmpe})_2\text{CrCl}_2]$.^{18,52} However, Berben demonstrated that a dinuclear Cr^I dinitrogen-bridged acetylide complex could be synthesized by mixing $[(\text{dmpe})_2\text{CrCl}_2]$ with stoichiometric LiC₂SiMe₃ and excess *n*-butyllithium; the latter acts as a reducing agent. Nitrogen dissolved in the solvents cap and bridge the reduced Cr(dmpe)₂(C₂R) moieties. The syntheses of **1** and **2** were adapted from Berben's procedure; we find that quantitative removal of LiCl from the reaction mixture requires pentane extraction followed by filtration through Celite.⁵³

Complexes **1** and **2** have been fully characterized structurally and spectroscopically. Despite the paramagnetism exhibited by these compounds (vide infra), resonances in the ¹H NMR spectra of **1** and **2** can be assigned on the basis of approximate integration (Supporting Information, Figure S6). For brevity, and because of the structural similarities between **1** and **2**, we will focus discussion on the $^3\text{Pr}_3\text{Si}$ analogue **2**. All characterization for **1** is presented in the Supporting Information.

Shown in Figure 2, the cyclic voltammogram obtained for **2** in THF shows two well-defined, reversible waves centered at -1.37 and -1.64 V (all potentials vs Fc⁺/Fc). The one-electron reversible redox waves centered at -1.64 and -1.37 V are assignable to mono- and dioxidation of the neutral compound to formally Cr^ICr^{II} and Cr^{II}Cr^{II} complexes, respectively. The peak-to-peak separations in the cyclic voltammograms imply a comproportionation constant for the reaction $[\text{RC}_2\text{Cr}^{\text{I}}(\mu\text{-N}_2)\text{Cr}^{\text{I}}\text{C}_2\text{R}] + [\text{RC}_2\text{Cr}^{\text{II}}(\mu\text{-N}_2)\text{Cr}^{\text{II}}\text{C}_2\text{R}]^{2+} \rightleftharpoons 2[\text{RC}_2\text{Cr}^{\text{I}}(\mu\text{-N}_2)\text{Cr}^{\text{II}}\text{C}_2\text{R}]^+$ as $\sim 10^{4.5}$, a value which suggests Robin–Day Class II behavior for the monocationic species.⁵⁴ Diethyl ethereal solutions of **2** can be cleanly oxidized by stoichiometric [Cp₂Co]⁺ or [Cp₂*Fe]⁺ to afford the one- and two-electron oxidized complexes **3** and **4**, respectively. Complete electrochemical characterization of all compounds can be found in the Supporting Information.

(51) The Ahlrichs DZ basis set was obtained from the TurboMole basis set library under <ftp://chemie.uni-karlsruhe.de/pub/basen>.

(52) Lopez-Hernandez, A.; Venkatesan, K.; Schmalle, H. W.; Berke, H. *Monatsh. Chem.* **2009**, *140*, 845–857.

(53) In the presence of chloride (from adventitious LiCl), over a period of hours, intensely colored solutions of oxidized **2** turn pale yellow, and crystals of $[(\text{Pr})_3\text{SiC}_2\text{Cr}^{\text{III}}\text{Cl}](\text{BAr}_4^{\text{F}})$ can be isolated. Details concerning the reactivity of these species are under investigation.

(54) Robin, M. B.; Day, P. *Adv. Inorg. Chem. Radiochem.* **1967**, *10*, 247–422.

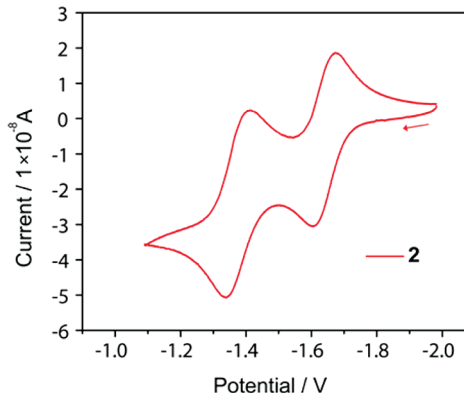


Figure 2. Cyclic voltammograms of the neutral dinuclear complex **2** obtained in THF.

The solid state IR spectra for all the dinitrogen-bridged complexes exhibit a single absorption in the acetylide stretching region. In redox-related **2–4**, the peak shifts higher in energy by 19 cm^{-1} with each successive oxidation. The solution Raman spectra of **2** and **4** show strong resonances for the dinitrogen symmetric stretch,⁵⁵ indicating that the homovalent complexes are stable and effectively centrosymmetric in solution.⁵⁶

X-ray Crystallography. The crystal structures of dinitrogen complexes **2–4** (Figure 3) reveal essentially octahedral coordination geometries around each chromium ion. Selected bond distances and angles are presented in Table 2. The acetylide and bridging dinitrogen ligands are located trans to each other while the equatorial positions are occupied by the two bidentate dmpe ligands. Viewed along the Cr–N–N–Cr axis, the four dmpe ligands are offset rotationally such that the methyl substituents for the phosphine ligands surrounding one Cr atom fit snugly between the methyl substituents for the dmpe ligands coordinated to the other Cr atom. Notwithstanding, steric interactions between the methyl substituents cause the dmpe ligands to distort slightly from the center of the molecule. The R–C≡C–Cr–N–N–Cr–C≡C–R skeleton is nearly linear. The N–N bond distance of 1.187(5) Å for **2** suggests that the bridging ligand is mildly activated with respect to free dinitrogen (1.0971(2) Å).⁵⁷ The averaged Cr–P bond distances for **2** are similar to those reported for *trans*-[Cr(dmpe)₂(CO)₂]BPh₄,⁵⁸ which represents the only structurally characterized monovalent [Cr(dmpe)₂] complex prior to Berben and Kozimor's report.¹⁸ The averaged Cr–N distance of 1.881(2) for **2** lies between the reported Cr–N distances observed for N₂-bridged zero-⁵⁹ and trivalent⁶⁰ chromium complexes. Skeletal bond distances and angles are very similar to

(55) MacKay, B. A.; Fryzuk, M. D. *Chem. Rev.* **2004**, *104*, 385–402.

(56) Attempts to collect Raman spectra of **3** have been thwarted by the propensity of **3** to undergo a reversible reaction upon irradiation with the 1064 nm incident laser. Dark green ethereal solutions of **3** turn golden brown upon insertion into the path of the laser; removal prompts the dark green color to reappear. We tentatively attribute this reactivity to reversible coordination of dinitrogen.

(57) Wilkinson, P. G.; Houk, N. B. *J. Chem. Phys.* **1956**, *24*, 528–534.

(58) Salt, J. E.; Wilkinson, G.; Motellalli, M.; Hursthouse, M. B. *J. Chem. Soc., Dalton Trans.* **1986**, 1141–1154.

(59) Denholm, S.; Hunter, G.; Weakley, T. J. R. *J. Chem. Soc., Dalton Trans.* **1987**, 2789–2791.

(60) Vidyaratne, I.; Scott, J.; Gambarotta, S.; Budzelaar, P. H. M. *Inorg. Chem.* **2007**, *46*, 7040–7049.

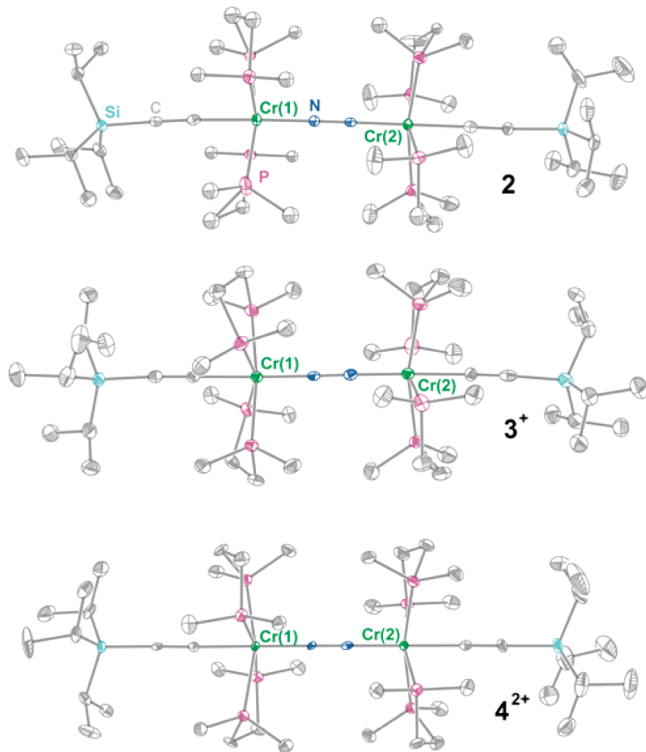


Figure 3. Crystal structures of the $[\text{Cr}_2(\mu\text{-N}_2)]^n+$ ($n = 0, 1, 2$) complexes in compounds **2**, **3**·1.5Et₂O and **4**·3.5THF, rendered with 40% ellipsoids. Green, violet, dark blue, light blue, and gray ellipsoids represent Cr, P, N, Si and C atoms, respectively. Hydrogen atoms, minor components of disordered atoms, charge balancing anions and solvent molecules are omitted for clarity. None of these complexes reside on sites of higher crystallographic symmetry.

those reported for the trimethylsilyl analogue:¹⁸ the N–N bond length for **2** is the same within experimental error, and the mean Cr–P distances differ by less than 0.01 Å.

Comparing the oxidized complex salts **3** and **4** to the neutral complex **2**, the Cr–P interatomic distances are the same within experimental uncertainties for **2** and **3** and are slightly longer for **4** (Table 2). The dicationic complex **4** shows Cr–P distances that are comparable to $[\text{Cr}^{\text{III}}\text{-}(\text{dmpe})_2\text{Cl}_2]\text{BPh}_4$,⁵⁸ and distances for **3** are intermediate between **2** and **4**. With the exception of the Cr–P bond distances, the structures are nearly superimposable despite the different formal oxidation states of the Cr ions. Significantly, we find that the Cr–N and N–N bond distances vary only slightly within this redox-related family.

Regarding monooxidized **3** specifically, we note only minor differences between the structures obtained at 100 and 296 K. First, where the low temperature structure contains diethyl ether solvate molecules, the high temperature structure exhibits void spaces. Second, the averaged Cr–P bond distances are the same for both Cr centers at 100 K (Cr(1)–P = 2.347(7) Å, Cr(2)–P = 2.35(1) Å), but are slightly different at the 1 σ estimated standard deviation⁶¹ at 296 K (Cr(1)–P = 2.365(9) Å, Cr(2)–P = 2.39(1) Å). Given the relatively large uncertainties in metric parameters and the difference in solvation, we do not find strong evidence for valence localization in the room temperature structure; however, bond

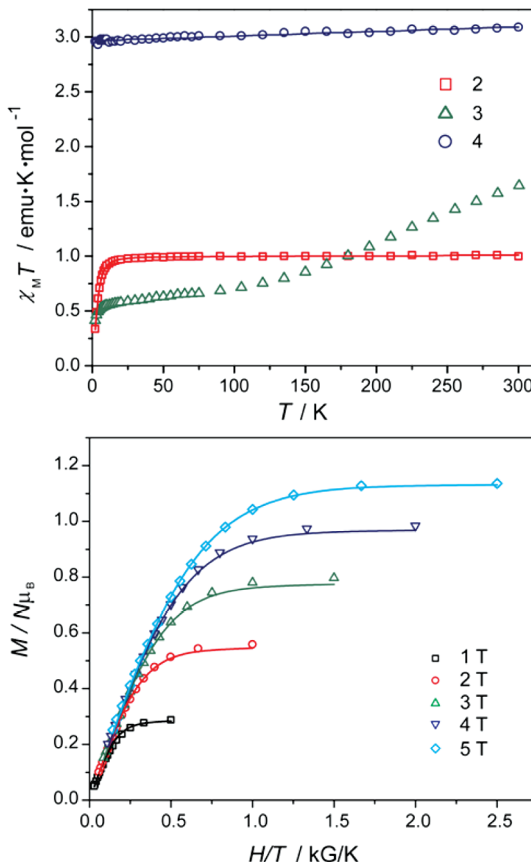


Figure 4. Top: temperature dependence of the magnetic susceptibility and best fits (solid lines) for compounds **2**, **3**, and **4**, obtained at a measuring field of 1000 G. Bottom: magnetization behavior and fit for compound **2**. See text for details of the fitting procedures.

distances in the low temperature structure are consistent with delocalization of chromium valence.

Magnetic Properties. Shown in Figure 4, the $\chi_M T$ product for **2** decreases only slightly upon cooling to $0.96 \text{ cm}^3 \cdot \text{K} \cdot \text{mol}^{-1}$ at 16 K, then drops off more precipitously to $0.34 \text{ cm}^3 \cdot \text{K} \cdot \text{mol}^{-1}$ at 2 K. Using julX⁴¹ to fit the susceptibility data with a spin Hamiltonian that incorporates a zero-field splitting (ZFS) parameter, the downturn in susceptibility below 16 K can be reproduced to afford a *D* value of $+8.34 \text{ cm}^{-1}$ and a *g* value of 1.99. In contrast, fitting the susceptibility data to a model where the formally Cr^I centers couple antiferromagnetically affords unreasonably large *g* values. See Supporting Information for details concerning alternative models. The magnetization plot for **2** (Figure 4, bottom) exhibits non-superposition of the isofield data, a hallmark of a magnetically anisotropic ground state. Fitting the magnetization data with ANISOFIT⁴² yields a ZFS parameter of *D* = $+8.22 \text{ cm}^{-1}$ with *g* = 1.95, values that are consistent with best fits to the magnetic susceptibility data.

Qualitatively, the susceptibility data for **4** is similar to that observed for **2**. At 300 K, the $\chi_M T$ product has a value of $3.09 \text{ cm}^3 \cdot \text{K} \cdot \text{mol}^{-1}$. This value hardly changes as the temperature is reduced, dropping to $2.95 \text{ cm}^3 \cdot \text{K} \cdot \text{mol}^{-1}$ at 2 K. Fits of this data to an *S* = 2 model afford a reasonable *g* value of 1.99. In contrast to **2**, the magnetic data for **4** does not appreciably decrease at low temperatures, and all the magnetization data collected at varying fields are superimposable upon the *S* = 2 Brillouin

(61) The bond distances are different at 1 σ , but are indistinguishable at the 3 σ level.

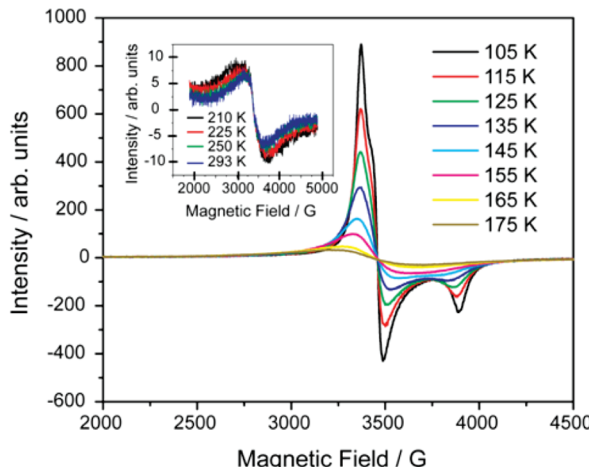


Figure 5. Solid state variable temperature EPR spectra of compound **3** (105–175 K). Inset: high temperature spectra of **3** (210–293 K).

function, indicating the absence of ZFS in the dioxidized compound (Supporting Information, Figure S9).

In contrast to the nearly temperature invariant behavior of **2** and **4**, the susceptibility data for complex **3** show a steady decrease in $\chi_M T$ upon cooling, from $1.64 \text{ cm}^3 \cdot \text{K} \cdot \text{mol}^{-1}$ at 300 K to $0.75 \text{ cm}^3 \cdot \text{K} \cdot \text{mol}^{-1}$ at 105 K, followed by a milder decrease to $0.57 \text{ cm}^3 \cdot \text{K} \cdot \text{mol}^{-1}$ at 16 K. Below 16 K, the susceptibility drops sharply to $0.42 \text{ cm}^3 \cdot \text{K} \cdot \text{mol}^{-1}$ at 2 K. As with **2**, the non-superposition of the isofield data in the reduced magnetization plot confirms the presence of ZFS (Supporting Information, Figure S9), but satisfactory fits using ANISOFIT have not been obtained, likely owing to the lack of a well-defined ground state (*vide infra*). The low temperature/high field magnetization appears to saturate at approximately $1.3 N\mu_B$,^{62,63} a value which is consistent with a mostly filled $S = 1/2$ ground state. The magnetization and low field susceptibility data agree within $0.02 \text{ cm}^3 \cdot \text{K} \cdot \text{mol}^{-1}$, and are slightly higher than what is predicted for an $S = 1/2$ ground state at low temperatures ($1.0 N\mu_B$ and $0.375 \text{ cm}^3 \cdot \text{K} \cdot \text{mol}^{-1}$ if $g = 2.00$). We note that the susceptibility and magnetization data obtained for all compounds, including **3**, are consistent from sample to sample.

X-band EPR spectra were collected for compounds **2–4** between 293 and 105 K to further investigate the magnetic properties of the complexes as well as to (attempt to) obtain independent measures of g values. Compounds **2** and **4** are effectively EPR-silent (Supporting Information, Figures S11 and S12). The spectra feature only minuscule signals at $g \sim 2$ which vary in intensity from sample to sample, consistent with the formation of trace impurities during sample preparation. The low signal-to-noise ratios in the spectra of **2** and **4** relative to **3** indicate that any paramagnetic impurities are not making significant contributions to the magnetic susceptibility data (Figure 4). Meanwhile, in the solid state spectrum for **3** obtained at 293 K (Figure 5), a faint, broad signal centered at $g_{\text{iso}} = 2.00$ is observed. As the temperature is lowered to about 175 K, the intensity of the signal begins to increase. At 155 K,

the signal begins to develop some rhombicity; at 105 K three resolved signals are observed at $g_{\perp} = 2.01$ and 1.96 and $g_{\parallel} = 1.74$. The appearance of the g_{\parallel} signal tracks with the susceptibility drop-off in the variable temperature magnetic data as well as the inflection point in the Weiss plot for **3** (Supporting Information, Figure S10).

Electronic Structure Calculations. To better correlate oxidation state changes to the observed structural and magnetic properties, we undertook a series of electronic structure calculations on **2–4**, including geometry optimization. To enforce proper ligand-field effects, Cr–P distances were constrained to experimental values. The computed metrics of the triplet and quintet states of **2** and **4**, respectively, are in substantial agreement with experiment (Table 2). Computed Cr–X bond distances are systematically long. We are able to computationally reproduce the observed relative insensitivities of the N–N and Cr–N distances to dioxidation. Angular metrics are in good agreement with the X-ray data.

The UKS⁶⁴ net spin density plots for **2–4** are presented in Figure 6. The parent complex **2** (Figure 6a) indicates orthogonal d– π^* character in the singly occupied orbitals of the low spin d⁵-d⁵ electronic configuration—hence a triplet ground state, in agreement with the computations of Berben and Kozimor. A higher lying singlet state, wherein the d– π^* orbitals are singlet coupled, is anticipated based on an O₂ bonding model. An $m_S = 0$ broken symmetry state solution is computed to be 17 kcal/mol above the triplet ground state. For reference, the ¹ Δ state of O₂ occurs 23 kcal/mol above the triplet ground state.⁶⁵ For **4**, the net spin density plot (Figure 6e) suggests oxidation occurs at each metal center, exposing orthogonal singly occupied d δ orbitals. The staggered orientation of the dmpe ligands causes the cloverleaf pattern of one d δ to line up with the nodal surface of the other when viewed down the Cr–Cr axis. A set of four mutually orthogonal d orbitals (two d δ , two d π) gives rise to a quintet ground state. A broken symmetry $m_S = 0$ state model is computed to occur at 14 kcal/mol above the quintet.

These spin-density based descriptions of **2** and **4** are supported by the fractionally occupied UKS spin natural orbitals. For **2** the d δ orbitals are nearly doubly occupied (Figures 7a and 7b) whereas for **4** (Supporting Information, Figures S18c and S18d) the d δ orbitals have occupancies near 1. Consistent with Berben and Kozimor's report, the highest significantly occupied natural orbitals for **2** (Figures 7e and 7f) display N–N π bonding and Cr–N π^* character. For **2**, the fractionally occupied UKS natural orbitals (Figures 7c, 7d, 7g, and 7h) are strongly suggestive of the first and second natural orbitals of a strongly correlated spin-paired bonding model for a pair of orthogonal Cr–N pi bonds. For **4**, a similar picture emerges; here the fractional occupancies are 1.88 and 0.12 (Supporting Information, Figures S18a, S18b, S18g, and S18h). Although natural orbital analysis does not provide orbital energies, the absolute orbital occupations of **2** and **4** are suggestive of the relative energies. The Cr δ orbitals, having the highest occupancies of 1.99 electrons, appear

(62) Kahn, O. *Molecular Magnetism*; Wiley-VCH: New York, 1993.

(63) This is not to be confused with the expected μ_{eff} for a single unpaired electron. As Kahn has noted, the Bohr magneton is better reserved as a unit of magnetization.

(64) Kohn, W.; Sham, L. J. *Phys. Rev.* **1965**, *140*, A1133–A1138.

(65) Huber, K. P.; Herzberg, G. *Constants of Diatomic Molecules*; Van Nostrand Reinhold: New York, 1979; Vol. 4.

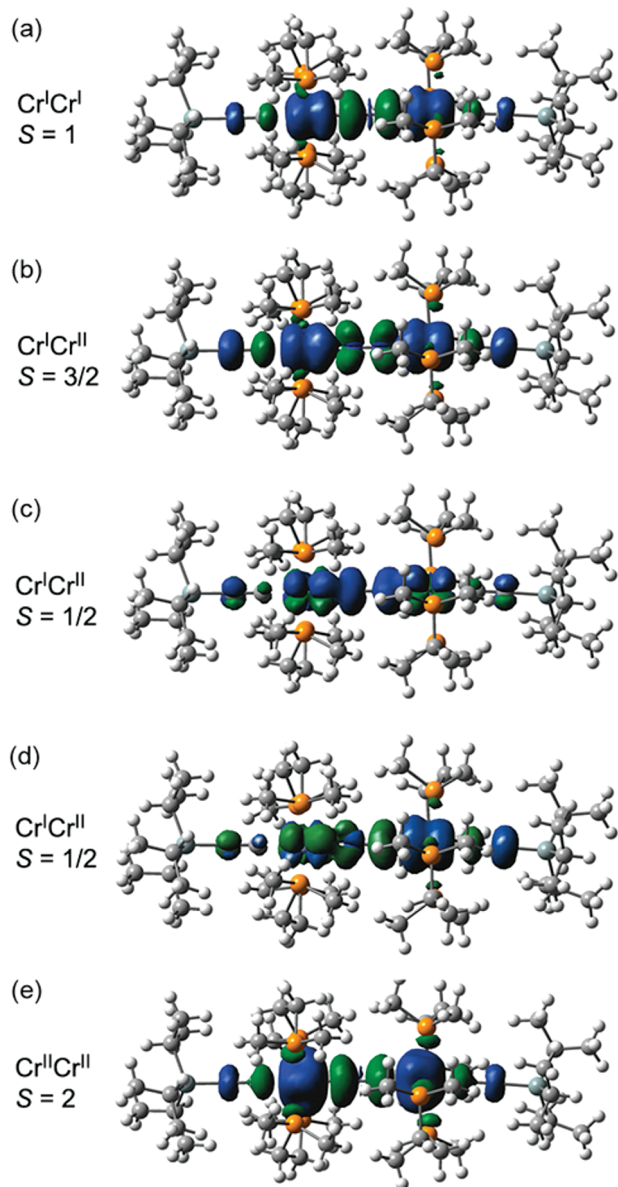


Figure 6. Net spin density plots (scaled at 0.0025 atomic units) for the (a) triplet ground state in **2**; (b) quartet (computed) ground state for **3**; (c) symmetrically delocalized doublet for **3**; (d) localized doublet for **3**; (e) quintet ground state in **4**. Blue surfaces correspond to net α spin density and green to net β spin density.

to be lowest in energy in **2** whereas the Cr–N π orbitals show the highest occupancies in **4**. By including dioxidized **4** in our study, we find that oxidation involves removal of an electron from each of the $d\delta$ orbitals in **2** and the highest occupied orbitals retain N–N π bonding character.

For the mixed-valent complex **3**, the B3LYP density functional theory (DFT) model computes the quartet state (Figure 6b) to be significantly lower in energy than the lowest doublet, in contrast with the variable temperature magnetic susceptibility data. A symmetrically delocalized doublet wherein orthogonal $d\pi$ orbitals are antiferromagnetically coupled is computed to arise at 16 kcal/mol (Figure 6c), and a localized state where excess α spin density is localized on one end is found at 6 kcal/mol (Figure 6d). The Cr–N–N–Cr metrics for **3** are not well described by a quartet B3LYP model: the Cr–N distance

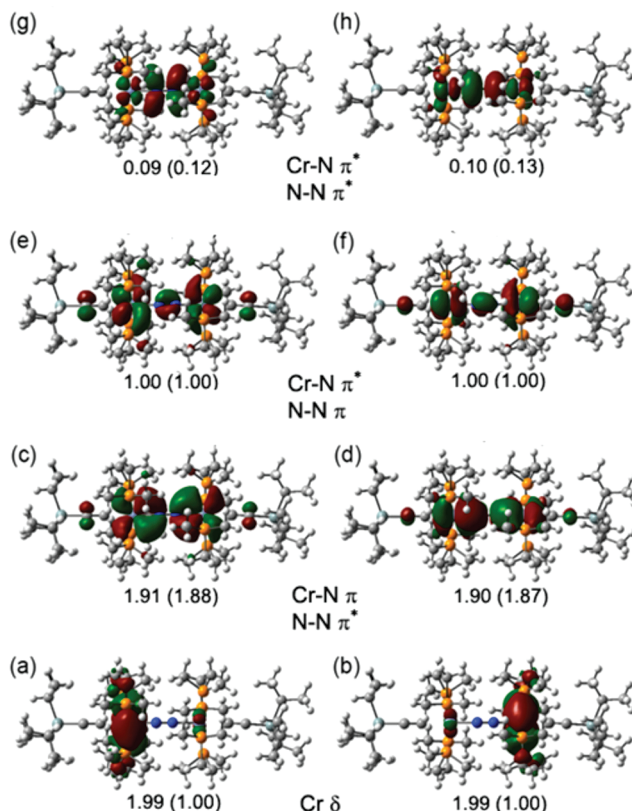


Figure 7. UKS frontier natural orbitals for **2** with corresponding electron occupancies. The electron occupancies for related orbitals in **4** are shown in parentheses.

is 0.16 Å long in **3** (compared to 0.05 Å long in **2** and **4**), the error in the N–N distance (0.04 Å)⁶⁶ is an order of magnitude larger than those found for **2** and **4**, and the computed N–N distance is short for **3** but long for **2** and **4**.

In contrast to the DFT model, we find the state averaged spectroscopy oriented restricted CI (CAS-SORCI) method⁶⁷ enjoys more success in accounting for the magnetic properties of the mixed valent compound **3**. The average field [9,11] CAS SCF computation on a model for **3** (**3***) finds a quartet ground state, followed by the second quartet at 2.45 kcal/mol, the lowest doublet at 2.23 kcal/mol, and the second doublet at 5.04 kcal/mol. Both doublets and quartets benefit from resonance stabilization. Because of the Fermi/exchange hole, there should be significantly more electron correlation for the doublets than for the quartets. The extra correlation of the SORCI places the doublets *lower* than the quartets. The second doublet is computed to occur 0.59 kcal/mol above the ground state doublet, and two quartet states reside at 1.45 and 2.81 kcal/mol above the ground state doublet. The CAS-SORCI total energy for the lowest doublet is -5394.834154395 hartree.

Discussion

Berben and Kozimor used the results of a UKS B3LYP study on the model complex $[(dpe)_4Cr^I_2(C_2H_2)(\mu-N_2)]$ (dpe = diphosphinoethane) to propose that oxidation of the di-nuclear Cr^I–Cr^I compound (removal of an electron from

(66) All structural comparisons related to **3** refer to the X-ray structure of **3**·1.5Et₂O.

(67) Neese, F. *J. Chem. Phys.* **2003**, *119*, 9428–9443.

each of the degenerate singly occupied molecular orbitals, SOMOs) should result in a weakened N–N bond and an increase in Cr–N bond character.¹⁸ This reasonable suggestion was based on the observation that the degenerate SOMOs each contained significant N–N π bonding character and significant Cr–N π^* character. The demonstrated electrochemical (CV) stabilities of the mono- and dioxidized species implied that bulk quantities of the species could be produced for interrogation. Indeed, in this work we find that mono- and dioxidized **3** and **4** can be synthesized from neutral **2** by simple stoichiometric addition of appropriate organometallic oxidants. However, a comparison between the crystallographically determined N–N and Cr–C bond distances in **2** and **4** indicates that there is no significant change in the bond lengths upon oxidation (Table 2).⁶⁸ This is in contrast to what one would expect with regards to the similarity of the model complex on which the original calculations were performed. In addition, the N–N stretching frequency increases when the neutral complex **2** is oxidized by two electrons to **4**. The shift to higher energies relative to the neutral complexes is opposite to the behavior expected if the N–N bond order were to decrease upon oxidation, as predicted by DFT calculations carried out on the neutral complex.¹⁸

On the basis of the structural, magnetic and computational results we have acquired, we offer the following explanation: dinitrogen “activation” occurs, but only at the time of the neutral dinuclear complex formation. The natural orbitals generated for **2** (Figure 7), as well as the Berben/Kozimor calculations, are consistent with the formation of Cr=N moieties. The formation of Cr=N-type interactions implies that the N≡N bond order has been reduced; the apparent mild activation derived from X-ray structural data may be masked by ancillary ligand steric considerations, for example, the relatively tight packing of the dmpe ligands on neighboring Cr centers. Then, as the calculations for **4** suggest (Supporting Information, Figure S18), subsequent oxidation of the neutral complex **2** does not follow Koopman’s theorem, a situation which is common for transition metal complexes. Upon oxidation, electrons are removed from the Cr d δ orbitals instead of d π orbitals, Cr–N π -bonding remains intact, and retention of this bonding leads to the computed variable occupation of the d δ orbitals and the observation of non-diamagnetic ground states as discussed below. If the computed natural orbital occupations for neutral **2** and dioxidized **4** indicate a switch in relative orbital energies, it is reasonable to expect that the d π and d δ orbitals in the intermediate complex **3** should be of nearly equal energies, which might afford novel magnetism.

Magnetic Properties. While it has been suggested that the N₂ ligand engenders (weak) antiferromagnetic coupling between metal centers in some cases,^{17,18,24} others have reported non-diamagnetic, high-spin ground states for dicobalt,²⁰ and dimolybdenum¹⁹ complexes. Münck and Bominaar have performed an extensive theoretical and Mössbauer study of on a diiron complex,²² and conclude that the high spin behavior observed there originates from strong direct metal–ligand antiferromagnetic coupling. A similar mechanism has been cited to account for the diamagnetism found in a Ni^I₂ complex.²⁴

(68) However, we note that the mono-oxidized compound **3** does show very slightly longer N–N and shorter Cr–N distances compared to neutral **2**.

For the neutral compound **2**, the room temperature magnitude of $\chi_M T$, 1.00 cm³·K·mol⁻¹ at 300 K, evokes an $S = 1$ ground state rather than two uncoupled low spin d⁵ centers (expected $\chi_M T \approx 0.75$ cm³·K·mol⁻¹), assuming a g value of 2 (Figure 4 and Supporting Information, Figure S8). The sharp downturn in susceptibility at low temperatures has been reasonably interpreted as weak antiferromagnetic coupling in the trimethylsilyl analogue,¹⁸ but it is also consistent with significant ZFS, which is often associated with triplet ($S = 1$) ground states.⁶⁹ Fits of the susceptibility and magnetization data are both consistent with a triplet system, whereas satisfactory fits based on metal–metal and metal–ligand antiferromagnetic coupling models could not be obtained. We also note here that the $S = 1$ ground state is consistent with our DFT calculations for **2** as well as Berben and Kozimor’s original electronic structure model. Antiferromagnetic coupling of spins in the neutral complex would lead to a singlet ($S = 0$) ground state.

Similarly, a larger-than-expected susceptibility value at high temperature for two uncoupled $S = 1$ centers (expected $\chi_M T \approx 2$ cm³·K·mol⁻¹, but 3.09 cm³·K·mol⁻¹ is observed) leads us to classify dioxidized compound **4** as having an $S = 2$ ground state. A satisfactory fit based on an $S = 2$ model is obtained for the susceptibility data for **4**. Unlike **2**, the lack of a significant decrease in the magnitude of $\chi_M T$ at low temperatures implies that ZFS is not present in **2**. Supporting this, the isofield data in the magnetization plot overlay the $S = 2$ Brillouin function (Supporting Information, Figure S9). Our electronic structure model does not provide an immediate explanation for the lack of ZFS: according to the calculations for **2** and **4**, there should be six electrons in the Cr–N π system, so orbital degeneracy should not change upon dioxidation; however, the orbital energies are shifted significantly upon oxidation, based on the fact that Cr d δ are now SOMOs, and thus we might reasonably expect different amounts of spin–orbit coupling for **2** and **4**, leading to different zero-field magnetic behavior. A detailed analysis of this interesting phenomenon is in progress.⁷⁰

The magnetic behavior found for **2** bears some resemblance to the triplet ground states observed in paramagnetic (C₄)²⁻-bridged complexes such as [I₂(dmpe)₄Mn₂(μ -C₄)].⁷¹ Theoretical calculations for those complexes reveal that the highest occupied molecular orbital (HOMO) is delocalized over the entire length of the bridging ligand. However, oxidation by two electrons of the formally d⁵-d⁵ [Mn^{II}₂(μ -C₄)] complex yields a diamagnetic d⁴-d⁴ complex. The diamagnetic ground state for the [Mn^{III}₂(μ -C₄)]²⁺ species has been attributed to a significant contribution of the cumulenic resonance structure to the overall bonding picture. The fact that **4** is paramagnetic indicates that the electronic structure of **2** must be significantly different from the previously reported diyne-bridged dinuclear complexes.

For a dinitrogen bridged iron-diketiminate complex, Münck and co-workers observe a high spin ground state

(69) *Physical Methods in Bioinorganic Chemistry*; University Science: Sausalito, 2000.

(70) Rappé, A. K.; Hoffert, W. A.; Shores, M. P. manuscript in preparation.

(71) Kheradmandan, S.; Heinze, K.; Schmalle, H. W.; Berke, H. *Angew. Chem., Int. Ed.* **1999**, 38, 2270–2273.

arising from a variable occupation of d orbitals because of N₂-induced Fe oxidation.²² They attributed these observations to strong direct antiferromagnetism between the iron and nitrogen centers. Bonding and direct antiferromagnetism are limiting models on a continuum. We would suggest an operational model wherein interactions that can be disrupted by conventional temperatures and magnetic fields constitute direct antiferromagnetic interactions; otherwise, they represent M–L bonding.

For mixed-valent **3**, we believe the temperature dependence of the susceptibility data, a gradual decrease of $\chi_M T$ from 300 to 16 K followed by a steeper drop at very low temperatures, is best understood as an incomplete quartet \rightleftharpoons doublet two-center spin equilibrium, where the doublet state is anisotropic. As with **2** and **4**, we cannot generate satisfactory fits to the data assuming weak exchange coupling of the two chromium spin centers: the room temperature $\chi_M T$ value is too high for uncoupled $S = 1$ and $S = 1/2$ spin centers ($1.375 \text{ cm}^3 \cdot \text{K} \cdot \text{mol}^{-1}$) would be predicted for $g = 2$), and best fits to an antiferromagnetic coupling model give unreasonable g values (see Supporting Information). EPR spectroscopy further supports the assignment of a spin-crossover event for mixed-valent **3**. Whereas the featureless signal seen at higher temperatures (Figure 5 inset) is typical for isotropic quartet spin systems,⁷² the intensification and development of anisotropy in the g value upon temperature reduction is consistent with a spin state change.^{73–75} Furthermore, the temperature dependence of the $g_{||}$ signal is synchronized with the magnetic susceptibility drop-off.

Similar spin-crossover behavior has been observed before in mixed-valent diruthenium complexes in which the metal atoms are directly bound to one another.^{76,77} Related, Bruce and co-workers have reported a diyne-bridged biradical diiron complex that exists in a thermally tunable mixture of singlet and triplet states.⁷⁸ To our knowledge, the magnetic behavior of **3** represents the first example of ligand-mediated two-center spin crossover event in a mixed-valent species. In sum, the magnetic behavior of compounds **2**, **3**, and **4** are consistent with extensive spin delocalization across the Cr–N–N–Cr backbone. Most significantly, the putative quartet \rightleftharpoons doublet transition is observed despite the fact that both homovalent complexes **2** and **4** show high spin (ferromagnetic) behavior at virtually all temperatures probed.

Electronic Structure of the Mixed-Valent Compound 3. The unprecedented magnetic properties of the mono-oxidized complex in **3** should be linked to the high spin/non-diamagnetic ground states of the homovalent compounds **2** and **4**, but also incorporate effects related to

electron transfer/mixed valency. Thus, a deeper examination of the electronic structure of **3** is warranted.

The experimental data we have acquired for **3** does not allow for a clear-cut determination of mixed valency character. Analysis of electrochemical data (Figures 2 and Supporting Information, Figures S1–S4) suggest partial electronic delocalization for **3** (Robin–Day Class II behavior).⁵⁴ From this, it should be possible to observe a difference in the stretching frequencies for the acetylidy ligands bound to the formally Cr^I and Cr^{II} centers; however, the IR spectrum for **3** shows a single acetylidy stretching resonance, suggesting that the Cr termini are equivalent on the IR time scale (10^{-13} s). Also, the Cr–ligand bond distances in the crystal structures of **3** are consistent with valence delocalization. The examination of the near-IR spectra of solutions of **3** in Et₂O shows no absorptions that could represent an IVCT band (Supporting Information, Figure S7), and Hush analysis reveals that the observed bandwidth for the absorption peak at 914 nm is far too narrow to represent a IVCT process.^{79,80} Intramolecular electron transfer rates have been correlated to the anisotropy in the g value of mixed-valent complexes ($\Delta g = g_{\perp} - g_{||}$), where trapped ($\Delta g > 1.5$) or detrapped ($\Delta g < 1.1$) states give rise to slow and fast electron transfer, respectively.⁸¹ For **3**, $\Delta g = 0.22$ at 105 K, which is consistent with a detrapped state, indicating that the odd electron is being shuttled between the Cr centers at a very fast rate ($>10^8 \text{ s}^{-1}$). Similar observation of valence delocalization across a dinitrogen bridge has been observed before in mixed-valent Os^{III}/Os^{II} complexes.⁸² In sum, whereas the electrochemical experiments suggest only partial electronic localization, structural, magnetic and spectroscopic data suggest that **3** possesses a delocalized electronic structure. This does not break new ground: others have noted that mixed-valent species can exhibit properties consistent with both localized and delocalized electronic structures, especially when multiple M–L–M orbital pathways can be involved.^{3,83,84}

As might be expected from the multifaceted experimental results, the electronic structure calculations for **3** also reveal complexity. In going from **2** to **4**, one electron is removed from a d δ orbital on each chromium center. It would be reasonable to surmise that for **3**, one electron is removed from one of the doubly occupied d δ orbitals in **2**, generating a set of three orthogonal singly occupied d orbitals and a resulting quartet ground state.⁸⁵ Indeed, the quartet state (Figure 6b) is computed to be significantly lower in energy than the lowest doublet.

- (72) Drago, R. S. *Physical Methods for Chemists*; 2nd ed.; Surfside: Gainesville, 1992.
- (73) Le Stang, S.; Paul, F.; Lapinte, C. *Organometallics* **2000**, *19*, 1035–1043.
- (74) Denis, R.; Toupet, L.; Paul, F.; Lapinte, C. *Organometallics* **2000**, *19*, 4240–4251.
- (75) Roué, S.; Le Stang, S.; Toupet, L.; Lapinte, C. *C. R. Chim.* **2003**, *6*, 353–366.
- (76) Angaridis, P.; Cotton, F. A.; Murillo, C. A.; Villagran, D.; Wang, X. *J. Am. Chem. Soc.* **2005**, *127*, 5008–5009.
- (77) Tara, J. B.; Cameron, T. S.; Donal, H. M.; Laurence, K. T.; Manuel, A. S. A. *Eur. J. Inorg. Chem.* **2007**, *2007*, 4021–4027.
- (78) Bruce, M. I.; Costuas, K.; Davin, T.; Ellis, B. G.; Halet, J.-F.; Lapinte, C.; Low, P. J.; Smith, M. E.; Skelton, B. W.; Toupet, L.; White, A. H. *Organometallics* **2005**, *24*, 3864–3881.

(79) At any rate, all the compounds studied here feature intense peaks between 900 and 950 nm; metal-to-ligand charge transfer or symmetry-allowed HOMO–SOMO transitions are more likely candidates for assignment based on literature precedent.

(80) Klein, A.; Lavastre, O.; Fiedler, J. *Organometallics* **2005**, *25*, 635–643.

(81) Lohan, M.; Ecorchard, P.; Ruffer, T.; Justaud, F.; Lapinte, C.; Lang, H. *Organometallics* **2009**, *28*, 1878–1890.

(82) Demadis, K. D.; El-Samanody, E.-S.; Coia, G. M.; Meyer, T. J. *J. Am. Chem. Soc.* **1999**, *121*, 535–544.

(83) Lapinte, C. *J. Organomet. Chem.* **2008**, *693*, 793–801.

(84) Creutz, C. In *Progress in Inorganic Chemistry*; Lippard, S. J., Ed.; Wiley: New York, 1983; p 1–73.

(85) Alternatively, one electron could be added to one of the singly occupied d δ orbitals in **4**, again generating a set of three orthogonal singly occupied d orbitals and a quartet ground state.

Unfortunately, this B3LYP DFT model does not correspond to experimental observations: among other things, **3** displays the magnetism of a ground state doublet with a thermally accessible quartet excited state, and appears to be symmetric according to X-ray and IR experiments.

The DFT model does not take into account resonance stabilization. For the present Cr–N–N–Cr mixed-valent compound **3**, a resonance-stabilized localization model would involve a resonance between the localized state of Figure 6d, (where beta (blue) spin is localized on the right) with its counterpart (where beta spin is localized on the left). Molecular symmetry is restored, accompanied by an energetic stabilization, by use of two resonating wave functions wherein the electron is placed successively on each Cr atom. Compound **3** minimally comprises a resonating 3-electron/3-orbital doublet active space, for which there are two orthogonal spin eigenfunctions: (a) two electrons are singlet paired and the third electron is added on to create a doublet ($\uparrow\downarrow\uparrow$), and (b) two electrons are triplet coupled and the third is added with opposite spin to create a doublet ($\uparrow\downarrow\downarrow$). *Spin unrestricted models such as UKS can only compute the average of these two spin eigenfunction states.* For **3** the second (triplet coupled) spin eigenfunction should be significantly favored, since one-center d-d exchange interactions approach 15 kcal/mol for first row transition metals, leading to a significant underestimation of the energy of the doublet state in **3** relative to the quartet. This extra lower-spin correlation is the accepted explanation for ground states that violate Hund's rule, as observed in organic chemistry.⁸⁶ Indeed, the more computationally demanding CAS-SORCI methods confirm this for a model of the mixed-valent complex in **3**. These results remind us that caution must be taken when choosing computational methods to describe the electronic structures of complex spin systems. A full account of the evolution in our computational methodology, as applied to the species described herein, will be offered presently.⁷⁰

Conclusion

We have described the preparation, structural and magnetic characterization, and electronic structures of a redox-related family of $[RC_2Cr(\mu-N_2)CrC_2R]^{n+}$ ($n = 0, 1, 2$) acetylides complexes. Magnetic measurements performed on the $n = 0$ and $n = 2$ complexes are indicative of high-spin ground states at room temperature, which contrasts with the antiferromagnetic model presented for the Me_3Si analogue of **1** and **2**.¹⁸ From the electronic structure calculations, the magnetic behaviors for neutral **2** and dioxidized **4** originate

(86) Hrovat, D. A.; Borden, W. T. *J. Mol. Struct.: THEOCHEM* 1997, 398–399, 211–220.

from the population of doubly degenerate Cr–N π bonding orbitals; this in turn pins the orientation of the SOMOs to achieve an electronic structure reminiscent of dioxygen. The formation of Cr=N-type interactions implies that the N≡N bond order has been reduced; the apparent mild activation derived from X-ray structural data may be significantly masked by ancillary ligand steric considerations. The increase in Cr–N bond character is not inconsistent with the strong direct metal–ligand antiferromagnetic coupling advanced by Münck and Bominaar findings, though we would classify this particular Cr–N interaction as a bond under our operational model.

Whereas an interpretation of previously reported DFT calculations performed on a model complex predict a weakened dinitrogen bond upon oxidation of the low-spin $d^5 Cr^I$ centers, we find that the Cr–N–N–Cr skeletal structures differ very little despite alteration of the formal Cr oxidation states. The results of the calculations performed on $[Pr_3SiC_2Cr(\mu-N_2)CrC_2Si'Pr_3]^{n+}$ suggest that the redox events proceeding from **2** to **4** are primarily metal-centered, which is perhaps not surprising if N_2 activation occurred only in the original formation of the neutral species. The mixed-valent $n = 1$ complex **3** exhibits magnetic behavior consistent with a thermally activated quartet \rightleftharpoons doublet two-center spin equilibrium. To our knowledge, this phenomenon has not been observed before in a mixed-valent system, and efforts to understand this behavior from a theoretical standpoint are ongoing.⁷⁰ Importantly, while the characterization of the neutral complex alone allows for reasonable interpretations of magnetic properties, a more complete understanding of the contributing factors is attainable only when all three complex oxidation states are considered.

The $[RC_2Cr(\mu-N_2)CrC_2R]^{n+}$ complexes offer numerous handles for experimental interrogation; in addition, their moderate sizes allow for rigorous calculations to be carried out with a minimum of size reduction. They ultimately offer promise as a model system to address fundamental questions of electronic structure. Moving forward, we will use these and related species as a platform to test theory development in the fields of mixed-valency and electron transfer, areas where current DFT methods find difficulty.

Acknowledgment. This research was supported by Colorado State University and the ACS Petroleum Research Fund (44691-G3). We thank Prof. C. M. Elliott for assistance with electrochemical simulations and helpful discussions.

Supporting Information Available: X-ray structural data (cif); full characterization of **1**, details of spectroscopic and electrochemical characterizations of other compounds, as well as the full reference 44 (pdf). This material is available free of charge via the Internet at <http://pubs.acs.org>.